City, University of London Institutional Repository

This is the accepted version of the paper.

This version of the publication may differ from the final published version.

City Research Online

1   **Title:** Estimating settlements due to TBM tunnelling

2   **Abstract**

3   Soft-ground Tunnel Boring Machines (TBM) are the preferred solution for construction of long tunnels

4   and linear infrastructure assets, especially in urban areas. TBMs allow the control of tunnel face stability,

5   minimizing effects on the surrounding ground. Unfortunately, existing methods for the assessment of

6   ground surface movements due to TBM tunnelling either utilise complex and computationally expensive

7   numerical analyses or rely on simplistic volume loss theories, which do not consider the characteristics

8   of the ground and TBM operation. This paper presents a simple formulation to estimate the immediate

9   surface settlement due to the applied TBM support pressure, based on an analogy with the hyperbolic

10   behaviour of stress-strain curves of soils. The maximum surface settlement and volume loss were the

11   variables chosen to describe the ground movement while the TBM face support pressure describes the

12   tunnel internal support pressure. Uncertainties due to the inherent variability of geotechnical parameters

13   were also considered, resulting in definition of lower and upper boundaries. Data from a series of

14   centrifuge test results, with and without tunnel face reinforcement by forepoles and a real scale TBM

15   case study were used to validate the proposed model. Presented analyses show that the proposed

16   model adequately represented observed settlement data.

17

20

1. Introduction

Tunnel Boring Machines (TBMs) for soft ground have become the preferred option for construction of long tunnels in urban areas. Despite the careful operation of TBMs, ground disturbance is inevitable . Leca and New (2007) show that ground movements are induced by tunnelling as a consequence of the development of plastic zone of the groundmass, which is initiated at the tunnel face and propagates into the ground. Even settlements of low magnitude might cause serviceability problems on nearby structures or pipelines (Vorster et al., 2005). Therefore, the estimation of ground movements due to tunnelling is of paramount importance.

Several approaches that do not consider the specific conditions of TBM excavations have been proposed to estimate ground movements, such as empirical methods (Attewell and Woodman, 1982; Celestino et al., 2000; Franza and Marshall, 2019; Jacobsz et al., 2004; New, 1991; Peck, 1969; Vorster et al., 2005), analytical solutions (Litwiszyn, 1957; Sagaseta, 1987; Pinto and Whittle, 2014; Verruijt and Booker, 1996), numerical methods (Avgerinos et al., 2018; Fargnoli et al., 2015; Komiya et al., 1999; Lee and Rowe, 1990; Wongsaroj et al., 2013) or physical modelling (Atkinson and Potts, 1977; Franza et al., 2019; Marshall et al., 2012; Meguid et al., 2008; Schofield, 1980).

Ground movements due to TBM tunnelling are largely associated with plastic behaviour of the groundmass. Therefore, the most common procedures to minimize ground movement are based on methods to stabilize the tunnel face against groundmass instability by applying internal support pressure in the excavation chamber (Mair and Taylor, 1997). The design approach based on controlling ground movements through tunnel face support has led to the development of several methods for the evaluation of excavation stability. These methods, however, do not provide estimations of ground movement. It is simply assumed that a stable excavation would not produce significant settlements. According to Guglielmetti et al. (2008), the main analytical approaches for assessing tunnel face stability are those proposed by: Anagnostou and Kovári (1994, 1996), based on the limit equilibrium method (LEM); Carranza-Torres (2004), based on the Caquot's lower-bound solution of cavity collapse for an elastoplastic Mohr-Coulomb material; and Leca and Dormieux (1990), which is based on the upper-bound solution of plasticity theory. Numerical analysis of TBMs, based mainly on the Finite Element Method, is also employed for evaluating the effect of TBM support pressure in controlling tunnel face stability (Kavvadas et al., 2017).

Despite the large number of methods available for evaluating tunnel face stability, there is a

51   limited number of methods for the quantitative estimation of ground surface movements due to TBM

52   tunnelling. The short-term analysis of ground response is generally expressed in terms of the maximum

53   surface settlement (S_{max}) and the volume loss (V_L) variables. Ground movement has been empirically

54   related to the stability ratio (N), defined by Broms and Bennermark (1967). Attewell et al. (1986)

55   presented a direct correlation between V_L and N. Macklin (1999) proposed a relationship to estimate V_L

56   based on the concept of Load Factor (L_F) introduced by Mair et al. (1981) using results of centrifuge

57   tests. Later, Atkinson (2007), also based on centrifuge tests, proposed a relation between L_F, V_L, and

58   the applied support pressure.

59   Osman et al. (2006) proposed a simplified closed-form solution, based on the upper-bound

60   theorem of plasticity, for the prediction of maximum surface ground settlement considering the applied

61   tunnel support pressure. A series of five centrifuge test analyses on plane-strain unlined tunnels in

62   kaolin clay was conducted to validate this formulation. They observed a close correspondence between

63   experimental observations and theoretical predictions for deep tunnels (C/D > 3) but poor correlations

64   for shallow tunnels (C/D < 3), with C and D defined as in Figure 1.

65   This brief literature background indicates that there is a need for the development of methods for

66   estimating ground movements due to TBM excavation. In this context, a simplified method based on

67   the general approach presented by Osman et al. (2006) is presented herein. The proposed method

68   relates maximum settlement and volume loss with support pressures using an analogy with the

69   hyperbolic behaviour of stress-strain curves of soils. The proposed approach considers both drained

70   and undrained conditions, but the validation analyses presented herein are limited to centrifuge test

71   under undrained conditions. Furthermore, the definition of lower and upper-bound are proposed to

72   address the inherent variability of soil properties.

73

74   **2. Proposed model for ground surface settlement**

75   Figure 1 shows a representation of a typical transverse surface settlement curve, S (mm), due to

76   excavation, at a sufficient distance behind the advancing tunnel face. Peck (1969) and later Attewell

77   and Woodman (1982) approximated this behaviour to that of a Gaussian probability density function,

78   as follows:

79    $$S = S_{\max} \exp\left(-\frac{y^2}{2i^2}\right)$$ 1.

80   where: S_{max} is the maximum surface settlement (mm); y is the transverse distance (m); i is the

81   point of inflection distance of the settlement trough (m). The value of S_{max} may be estimated by

82   integrating Eq. 1 from minus to positive infinity, resulting in:

83    $$S_{max} = \frac{AV_L}{i\sqrt{2\pi}}$$ 2.

84   where: V_L is the volume loss (%) and A is the cross-sectional area of the tunnel (m^2). In general, this

85   approximation has been well accepted for its simplicity.

86   The groundmass displacement along the longitudinal direction (Figure 2) may be categorized as:

87   ▪ Face loss (zone "a" in Figure 2): ground movement towards the tunnel face due to stress relief.

88   For TBMs, this is normally associated with a low face pressure;

89   ▪ Shield loss (zone "b" in Figure 2): ground deformation around the shield due to over-cutting

90   edge combined with a misaligned TBM displacement that may result in radial ground

91   movements and soil shearing;

92   ▪ Tail void loss and lining loss (zone "c" in Figure 2): the first is due to the gap between the tail of

93   the shield and the final precast lining and the second is associated with the deflection of the

94   lining as the ground pressure increases as a consequence of soil closure on the lining. For

95   tunnels lined with thick pre-cast concrete segments, this is usually considered a minor source

96   of ground displacement; and

97   ▪ Consolidation (zone "d" in Figure 2): ground displacement due to a new pore-water pressure

98   distribution resulting from changes in the drainage conditions.

99   When the excavation is made in an uncontrolled manner, larger movements are observed, and

100   their mathematical modelling becomes more difficult due to erratic deformation patterns. However,

101   ground displacements may be minimized when tunnelling is performed in a highly controlled manner.

102   Settlements due to TBM excavation may be controlled by the continuous application of active support

103   pressure given by the TBM face support pressure and grout injection pressure (Guglielmetti et al., 2008;

104   Maidl et al., 2012; Mair, 2008; Mollon et al., 2013).

105   The first three settlement categories (i.e., zones a, b, and c) result in the "immediate" settlement

106   that occurs as the TBM face moves ahead of the measurement point. This paper deals only with the

107   immediate settlements during TBM tunnelling, in conditions that are predominately considered as

108   undrained but may, in highly permeable materials, occur under drained conditions.

109

110   2.1 Immediate surface settlement curve

111   Based on centrifuge test results, Atkinson (2007) presented a conceptual model of groundmass

112   response due to TBM tunnelling. Figure 3c shows a schematic representation of that model, expressed

113   in terms of the expected behaviour of immediate surface settlement due to the applied TBM support

114   pressure. During tunnelling, if the applied TBM support pressure, P, is equal to the estimated initial

115   support pressure for tunnel face stability, P_0, the surface settlement should be negligible. The initial

116   portion of the settlement curve corresponds to predominantly elastic behaviour. The onset of plastic

117   behaviour is identified as the settlement curve approaches the asymptote given by P_{min}. Relatively larger

118   settlements or even face collapse may occur when the applied TBM support pressure reaches a

119   minimum value, P_{min}, which is not necessarily zero.

120   In order to represent mathematically the general behaviour shown by Atkinson (2007), a model

121   selection analysis has been performed by Franco (2019). The statistical results indicated that a

122   hyperbolic function, similar to the stress-strain relationship (Figure 3d) proposed by Duncan and Chang

123   (1970), provides best results among the tested models. This formulation is based on the family of

124   hyperbolic equations, as follows:

125    $$\left(\sigma_1 - \sigma_3\right) = \frac{\varepsilon}{a + b\varepsilon}$$ 3.

126   where: σ_1 and σ_3 are the major and minor principal stresses, ε is the axial strain, and a and b are best-

127   fit parameters. The hyperbolic equation was used to express the relationship between the tunnel

128   pressure support variables shown in Figure 3c, as follows:

129    $$\left(\frac{S_{max}}{D}\right) = \frac{a_S\left(P_0 - P\right)}{b_S\left(P_0 - P\right) - 1}$$ 4.

130   where: S_{max} is the maximum surface settlement (mm); D is the tunnel diameter (mm); P is the applied

131   TBM support pressure (kPa); P_0 is the estimated initial TBM support pressure for face stability (kPa),

132   corresponding to null displacements, and a_S and b_S are best-fit parameters.

133   The value of P_0, applied along the tunnel axis, may be estimated based on the limit equilibrium

134   method (Anagnostou and Kovári, 1994, 1996) or based on limit analysis approaches (Carranza-Torres,

135   2004; Davis et al., 1980), among other methods reviewed by Guglielmetti et al. (2008). Note that,

136   depending on the adopted approach, P_0 is estimated by considering different parameters, such as the

137 tunnel geometry, the unit weight of the material, the coefficient of lateral earth pressure at rest (k_0); and

138 the shear strength parameters. Regarding the parameter k_0, Franzius et al. (2005) indicated that a

139 higher value of $k_0 = 1.5$ leads to generate widest settlement trough with too small maximum settlement

140 while a lower value of $k_0 = 0.5$ generates a narrower settlement trough with increased vertical

141 settlement. This analysis indicated that adopting extreme values of k_0 produce minor impact on the

142 estimation of the surface settlement magnitudes and profile. Note also that the tunnel diameter is

143 considered by means of a normalized variable used in Eq. 4.

144 The initial slope of the proposed settlement curve is obtained by taking the limit of the curve

145 derivative as P approaches P_0:

146 $$\frac{\partial}{\partial P}\left(\frac{S_{max}}{D}\right)\Bigg|_{P \to P_0} = a_S \qquad\qquad 5.$$

147 The asymptotic value of the ultimate stress difference $(P_0 - P)_{ult}$ may be determined by

148 rearranging Equation 4 and taking the following limit of S_{max}:

149 $$\lim_{S_{max} \to \infty}\left(\frac{S_{max}}{b_S S_{max} - a_S D}\right) = (P_0 - P)_{ult} = \frac{1}{b_S} \qquad\qquad 6.$$

150

151 2.2 Relationships between model parameters and geotechnical properties

152 Based on Equation 5, the following relationships are proposed for the estimation of the parameter

153 a_S, in the drained and undrained conditions in Equations 7 and 8, respectively:

154 $$a_S = 1\big/E_{ur}' \qquad\qquad 7.$$

155 $$a_S = 1\big/E_{ur} \qquad\qquad 8.$$

156 where: E_{ur}' and E_{ur} are the unloading-reloading elastic moduli (kPa) for drained and undrained

157 conditions, respectively.

158 Figure 3 presents an analogy between a triaxial loading test and the stress path due to TBM

159 tunnelling. Tunnel construction using a TBM often produces a reduced triaxial extension path, which is

160 the reverse form of a conventional triaxial compression. The groundmass may be brought to a state of

161 development of plastic zone by keeping the grout pressure constant, equal to P_0, and decreasing the

162 face pressure to a value equal to P_{min}, as shown in Figure 3e. The asymptotic value $(P_0 - P)_{ult}$ may be

163 related to the stress difference at failure $(P_0 - P_{min})$ using a constant failure ratio R_f inspired in the ratio

164   proposed by Duncan and Chang (1970):

165      $\left(P_0 - P_{\min}\right) = R_f^* \left(P_0 - P\right)_{ult}$ 9.

166   where: $R_f^* = R_f/(C/D)$. This definition of R_f^* allows the consideration of the influence of the ratio between

167   tunnel cover and diameter (C/D).

168   Assuming that P_{min} and P_0 are principal stresses and considering a limit state defined by the

169   Mohr-Coulomb envelope, the following expressions for ($P_0 - P_{min}$) are obtained for drained and

170   undrained conditions in Equations 10 and 11, respectively:

171      $\left(P_0 - P_{\min}\right) = \dfrac{2c'\cos\varphi' + 2\left(P_0 - u_{w0}\right)\sin\varphi'}{1 + \sin\varphi'}$ 10.

172      $\left(P_0 - P_{\min}\right) = 2S_u$ 11.

173   where: c' is the effective cohesion (kPa); φ' is the effective friction angle (deg.); u_{w0} is the pore-water

174   pressure at the tunnel axis (kPa); and S_u is the undrained shear strength (kPa).

175   Combining Equations 6, 9, 10, and 11, the following expressions are obtained for the parameter

176   b_S in the drained and undrained conditions, in Equations 12 and 13, respectively:

177      $b_S = \dfrac{1 + \sin\varphi'}{2c'\cos\varphi' + 2\left(P_0 - u_{w0}\right)\sin\varphi'} R_f^*$ 12.

178      $b_S = \dfrac{1}{2S_u} R_f^*$ 13.

179   The proposed simplified approach may also be used in terms of volume loss (V_L). According to

180   Atkinson (2007), V_L is defined as the ratio between the volume of over-excavated material and the

181   tunnel volume per unit distance. Similar to volumetric strain, volume loss is a dimensionless variable.

182   No relation is assumed between these two parameters, since in undrained conditions volumetric strain

183   is null while volume loss is not. The hyperbolic equation may be presented, in terms of volume loss V_L,

184   as follows:

185      $V_L = \dfrac{a_V\left(P_0 - P\right)}{b_V\left(P_0 - P\right) - 1}$ 14.

186   In a similar manner, the parameters a_V and b_V may be determined based on the elastic modulus

187   and on the limit state, for both drained and undrained conditions, as shown in Eqs. 6, 7, 12, and 13.

188   The equations in terms of V_L will not be used herein and only the model for S_{max} will be evaluated,

189   exclusively for the undrained condition. It is important to note that the proposed formulation relies on a

190   simplified representation of the complex groundmass stress distribution near the tunnel. Therefore, the

191   procedure proposed herein must be considered semi-empirical.

192

193   2.3 Dealing with the variability of input parameters

194   Some attention has been directed in the past towards the evaluation of how inherent groundmass

195   variability results in scattered ground displacements (Suwansawat and Einstein, 2006; Fargnoli et al.,

196   2013). The variability of geotechnical parameters and ground profile stratigraphy constitute a major

197   source of uncertainty for the assessment of ground movements in TBM tunnelling projects. Thus, an

198   appropriate description of these uncertainties is necessary (Kulhawy, 1992; Phoon and Kulhawy, 1999).

199   This section presents a simplified approach for the evaluation of the uncertainty of the settlement

200   curve model proposed herein. The indicated procedure is based on the approach proposed by Zhai and

201   Rahardjo (2013), using lower and upper-bound settlement curves. According to Kool et al. (1987), the

202   bounds of a model are directly correlated to the confidence limits of the input parameters. For this study,

203   the parameters a_S and b_S are assumed to be represented by the log-normal probability density function.

204   The lower and upper-bounds are defined by estimating the 10th and 90th percentiles of the probability

205   density function of each variable.

206   The physical meanings of the parameters a_S and b_S have been clearly defined and their

207   behaviour with respect to S_{max} is exemplified in Figure 4. If each variable is analysed separately, the

208   higher the values of a_S and b_S, the higher the absolute value of S_{max}. Therefore, the lower and upper

209   bounds of the settlement curve should be defined by specific combinations of a_S and b_S, as follows:

210
$$\left(\frac{S_{max}}{D}\right)_{upper-bound} = \frac{a_{S90}\left(P_0 - P\right)}{b_{S90}\left(P_0 - P\right) - 1}$$
15.

211
$$\left(\frac{S_{max}}{D}\right)_{lower-bound} = \frac{a_{S10}\left(P_0 - P\right)}{b_{S10}\left(P_0 - P\right) - 1}$$
16.

212   where a_{S90} and b_{S90} correspond to the 90th percentile and a_{S10} and b_{S10} correspond to the 10th percentile.

213   From a practical point of view in the tunnelling industry, the above approach might be considered

214   as complementary tool to be used in the protocol of tunnel excavation for defining the attention and

215   alarm limits of support pressure likely to occur during tunnelling as well as the immediate settlements

216   that the support pressure might induced.

217

218   **3. Analysis of centrifuge tests**

219   The following section presents the analysis of previously published results of centrifuge tests carried

220   out in undrained conditions, with and without the reinforcement of the tunnel face by forepoles. The

221   hyperbolic model (Eq. 4) is used to evaluate surface settlements as a function of support pressure.

222   Table 1 summarizes the features of each reference centrifuge test result collected from the literature.

223   Basic input information regarding the geometry of each centrifuge model and the geotechnical

224   properties are indicated. Unfortunately, only one reference presents information regarding the

225   unloading-reloading total elastic modulus, E_{ur}.

226   Figures 5 and 6 show experimental and modelling results of the centrifuge tests carried out by

227   Lee and Rowe (1989) and Osman et al. (2006), all without tunnel face reinforcement. A value of P_0 of

228   130 kPa was considered for each test. The tests involved different values of overburden depth (C) and

229   tunnel diameter ratio (C/D). Table 2 presents the best-fit values of a_S and b_S, obtained from nonlinear

230   regression analyses. The values of number of data points (n) and standard error (SE) for each variable

231   are also presented for each test. The values of coefficient of determination (R^2) and of Root Mean

232   Square Error (RMSE) indicate excellent agreement between the experimental data and the model, with

233   R^2 values ranging between 0.942 and 0.995.

234   Figure 7 shows a series of eight two-dimensional plane strain centrifuge model tests performed

235   by Divall et al. (2016). These tests were designed to investigate how forepoles affect the plastic collapse

236   mechanism surrounding a tunnel excavation in stiff clay. These results allow the evaluation, using the

237   proposed model, of how different forepole arrangements may artificially improve the soil around tunnel

238   and might affect the surface settlement behaviour. However, a detailed analysis of the behaviour of the

239   forepoles themselves is beyond the scope of this paper.

240   Divall et al. (2016) simulated the excavation by reducing the pressure, starting from an average

241   initial support pressure of 211 kPa. However, the test results indicated negligible ground response up

242   to a support pressure of 160 kPa, probably because P_0 was estimated as a function of the original soil

243   condition (i.e., without the influence of forepoles). To address this inconsistency, the formulation

244   proposed by Broms and Bennermark (1967) was employed:

245 $$N = \frac{\gamma(C + D/2) + \sigma_S - \sigma_T}{S_u}$$ 17.

246 where: γ = 17.5 kN/m³ (Divall, 2013); σ_S = 0 is the surface surcharge pressure; S_u = 30 kPa; and σ_T =

247 P_0.

248   Sensitivity analyses showed that values of N = 2 and P_0 = 160 kPa represented adequately the

249 centrifuge data. Therefore, a value of P_0 = 160 kPa was assumed in the modelling exercises presented

250 herein. Figure 7 shows, for all centrifuge arrangements, that the proposed model agrees with the test

251 results. The obtained coefficients of determination were higher than 0.99 for five out of eight tests.

252   Table 2 presents a comparison between the geotechnical parameters reported by the original

253 references and the respective values estimated using Eqs. 8 and 13 and the best-fit parameters for Eq.

254 4. The adopted value of R_f was 0.9 for all the tests with clays. Lee and Rowe (1989) are the only

255 reference that presents the value of E_{ur}, which is in close agreement with the model prediction.

256 Regarding S_u, most measured values were adequately predicted, with a maximum relative error of 15%.

257 The lower agreement observed for tests FP4, FP5 and FP7 from Divall et al. (2016) may be explained

258 by the higher values of surface settlement as collapse approaches, with a support pressure below 20

259 kPa. This is an obvious indication that the arrangements of forepoles may contribute to reinforce the

260 soil around the excavation. A Pearson correlation analysis of measured and predicted values of E_{ur} and

261 S_u, especially from the tests results performed by Divall et al. (2016), showed a correlation of r = 0.6149,

262 which indicates a moderate tendency for correlation. The lack of a strong correlation might be attributed

263 to the fact that the soil was artificially improved by the addition of forepoles.

264   The new formulation provided an accurate fitting of the ground surface movement with the

265 applied TBM support pressure as well as a consistent estimation of geotechnical parameters. Even

266 though the analyses with the tunnel face reinforced by forepoles are mainly used in practice with open

267 face tunnelling and not for TBMs, the formulation also demonstrates, in terms of the predicted values

268 of equivalent S_u, the effectiveness of the forepoles as soil reinforcement around a tunnel heading.

269

270 **4. Case study – Line 5 of São Paulo Metro**

271 The proposed procedure for incorporating the uncertainty of input parameters in the evaluation of

272 settlement curves has been applied to a case study. The tunnel project corresponds to a 11.5 km long

273 new extension of Line 5 of Sao Paulo Metro, located in the densely populated south region of the city

274   of Sao Paulo, Brazil (Figure 8). The new extension involves the construction of eleven stations and

275   thirteen ventilation shafts, among other structures and facilities. The line extension was excavated by

276   three Earth Pressure Balance (EPB) machines, two small EPB machines of 6.90 m in diameter, for two

277   single track tunnels between Adolfo Pinheiro and Eucalipto stations, and one large EPB machine of

278   10.60 m in diameter, for a double track tunnel between Eucalipto and Chacara Klabin stations. The

279   case study presented herein concerns the tunnel excavation by the larger EPB machine, specifically,

280   in a 670 m stretch of the tunnel line, located between Hospital Sao Paulo (HSP) and Santa Cruz (SCR)

281   stations. The tunnel cover depth in this section is of 24.35 m.

282   In terms of site geology, the line in this section crosses the Resende Formation, which comprises

283   basal and sedimentary units of the Taubaté Group from the Eocene Period. It consists of a system of

284   alluvial beds associated with the fluvial plain of intertwined rivers. This formation comprises two main

285   lithofacies. The first lithofacy corresponds to the proximal alluvial beds, located in the vicinity of the

286   contact with the basement, composed of polymitic conglomerates, interdigitated with sandstones and

287   sandy mudstones. The second lithofacy corresponds to the alluvial beds in distal position associated to

288   intertwined rivers, with occurrence of sandstones intercalated with mudstones. Detrital smectites

289   (argillomineral of the expansive type) are present, which are considered as indicators of climatic semi-

290   aridity and ineffective drainage.

291   The cover to diameter ratio (C=D) is constant along the tunnel stretch, with a value of 2.30.

292   Further details about this case study are presented by Franco et al. (2019).

293   Table 3 shows the observed maximum surface settlements (S_{max}) and applied TBM support

294   pressures (P) for each of the nineteen monitoring cross-sections. A relatively high variability is observed

295   for S_{max}, which was expressed in terms of the coefficient of variation (CoV). Franco (2019) performed

296   an analysis for the estimation of P_0 by following the limit equilibrium procedures proposed by

297   Anagnostou and Kovári (1994) and considering drained conditions. The groundmass has four different

298   soil types forming six layers, each layer with variable thickness. The values of C and D are 24.35 m and

299   10.60 m, respectively. The estimated value of P_0, in terms of total stress, was 308 kPa. Figure 9 and

300   Table 4 show the tunnel model geometry, and the mean soil property values, respectively, considered

301   in the case study for the estimation of P_0.

302   Figure 10 shows the best-fit results using the proposed model. The best-fit values for parameters

303    $D.a_S$ and b_S, obtained based on the monitored data, were equal to 0.02550 mm/kPa and 0.00285 1/kPa,

304 respectively. Figure 10 also shows the lower and upper-bound curves of the proposed model,

305 expressed in terms of the 10th and 90th percentiles, as proposed in Equation 18. Values of CoV between

306 10% and 46% were used to illustrate the variability of the model according to the variability of S_{max}

307 presented in Table 3. A value of CoV of 46% provides an adequate estimation of the lower and upper

308 bounds of the observed values. Therefore, the proposed model may be an acceptable indicator for

309 defining the limits in which soil variability affects the development of ground surface response during

310 TBM tunnelling.

311

5. Concluding remarks

313 In this paper a simple and practical model for the estimation of ground surface settlements due to TBM

314 tunnelling has been proposed, for both drained and undrained conditions. A series of centrifuge test

315 analyses was used to validate the proposed model. Furthermore, the case study of the new extension

316 of Line 5 of Sao Paulo metro was used to exemplify the determination of the settlement curve in

317 statistical terms, using lower and upper bounds.

318 The physical meaning of the model parameters, a_S and b_S, was demonstrated. In addition, an

319 alternative procedure for the estimation of these parameters was proposed, based on the soil stiffness,

320 shear strength, and initial tunnel support pressure. This semi-empirical estimation procedure is based

321 on an analogy between the stress states in the tunnel cavity and in triaxial tests. The parameter

322 estimation procedure depends on the tunnel cross- section that is under analysis. Therefore, to consider

323 P_0 along a tunnel stretch, the soil stratification must be constant, and the mean values of geotechnical

324 parameter should be considered along the tunnel path, for the ease of calculation.

325 The proposed approach was verified for geometrical conditions in which C/D < 3. Centrifuge tests

326 performed by Lee and Rowe (1989) and later by Osman et al. (2006) for C/D > 3 show that the

327 settlement curve presents a second inflection point, which may not be adequately represented by the

328 hyperbolic curves. Therefore, the formulation proposed herein should be applied with greater care for

329 deeper tunnels, with C/D > 3.

330 The proposed model offers a valuable tool for TBM tunnelling projects incorporating the support

331 pressure in the calculation of the tunnelling impact. In addition, the input parameters are based on

332 relatively simple standard tests. Finally, it is important to note that the proposed approach can be used

333 to derive lower and upper limits in order to consider the complexity and large number of variables that

334   affect groundmass response.

335

340

341   **References**

342   Anagnostou G and Kovári K (1994) The face stability of slurry-shield-driven tunnels. Tunnelling and

343   Underground Space Technology 9(2): 165 – 174.

344   Anagnostou G and Kovári K (1996) Face stability conditions with earth-pressure-balanced shields.

345   Tunnelling and Underground Space Technology 11(2): 165 – 173.

346   Atkinson J (2007) The mechanics of soils and foundations. CRC Press.

347   Atkinson JH and Potts DM (1977) Subsidence above shallow tunnels in soft ground. Journal of

348   Geotechnical and Geoenvironmental Engineering 103 (Proc. Paper 11318 Proceeding).

349   Attewell B and Woodman P (1982) Predicting the dynamics of ground settlement and its derivatives

350   caused by tunneling in soil 15(8): 13–22.

351   Avgerinos V, Potts DM, Standing JR and Wan MSP (2018) Predicting tunnelling-induced ground

352   movements and interpreting field measurements using numerical analysis: Crossrail case study at

353   hyde park. Géotechnique 68(1): 31–49.

354   Broms BB and Bennermark H (1967) Stability of clay at vertical openings. Journal of Soil Mechanics &

355   Foundations Div.

356   Carranza-Torres C (2004) Computation of Factor of Safety for Shallow Tunnels using Caquot's Lower

357   Bound Solution. Technical report, Technical Report for Geodata.

358   Celestino T, Gomes R and Bortolucci A (2000) Errors in ground distortions due to settlement trough

359   adjustment. Tunnelling and Underground Space Technology 15(1): 97 – 100.

360   Davis EH, Gunn MJ, Mair RJ and Seneviratine HN (1980) The stability of shallow tunnels and

361   underground openings in cohesive material. Géotechnique 30(4): 397–416.

362   Divall S (2013) Ground movements associated with twin-tunnel construction in clay. PhD thesis, City

363   University London.

364   Divall S, Taylor RN and Xu M (2016) Centrifuge modelling of tunnelling with forepoling. International
365   Journal of Physical Modelling in Geotechnics 16(2): 83–95.

366   Duncan JM and Chang CY (1970) Nonlinear analysis of stress and strain in soils. Journal of Soil
367   Mechanics & Foundations Div.

368   Fargnoli V, Boldini D and Amorosi A (2013) Tbm tunnelling-induced settlements in coarse-grained soils:
369   The case of the new milan underground line 5. Tunnelling and Underground Space Technology 38:
370   336 – 347.

371   Fargnoli V, Gragnano C, Boldini D and Amorosi A (2015) 3d numerical modelling of soil–structure
372   interaction during epb tunnelling. Géotechnique 65(1): 23–37.

373   Franco V (2019) Mathematical and probabilistic modeling approach for estimation of surface
374   settlements due to TBM tunneling. PhD thesis, Department of Civil and Environmental Engineering,
375   Universidade de Bras´ılia, DF, Brasília, 159p.

376   Franco VH, de F.N. Gitirana Jr. and de Assis AP (2019) Probabilistic assessment of tunneling-induced
377   building damage. Computers and Geotechnics 113: 103097.

378   Franza A and Marshall AM (2019) Empirical and semi-analytical methods for evaluating tunnelling-
379   induced ground movements in sands. Tunnelling and Underground Space Technology 88: 47 – 62.

380   Franza A, Marshall AM and Zhou B (2019) Greenfield tunnelling in sands: the effects of soil density and
381   relative depth. Géotechnique 69(4): 297–307.

382   Franzius JN, Potts DM and Burland JB (2005). The influence of soil anisotropy and K_0 on ground surface
383   movements resulting from tunnel excavation. Géotechnique, 55 (3): 189–199.

384   Guglielmetti V, Grasso P, Mahtab A and Xu S (2008) Mechanized Tunnelling in Urban Areas: Design
385   methodology and construction control. Taylor & Francis.

386   Jacobsz SW, Standing JR, Mair RJ, Hagiwara T and Sugiyama T (2004) Centrifuge modelling of
387   tunnelling near driven piles. SOILS AND FOUNDATIONS 44(1): 49–56.

388   Kavvadas M, Litsas D, Vazaios I and Fortsakis P (2017) Development of a 3d finite element model for
389   shield epb tunnelling. Tunnelling and Underground Space Technology 65: 22 – 34.

390   Komiya K, Soga K, Akagi H, Hagiwara T and Bolton MD (1999) Finite element modelling of excavation
391   and advancement processes of a shield tunnelling machine. SOILS AND FOUNDATIONS 39(3):
392   37–52.

393   Kool J, Parker J and van Genuchten M (1987) Parameter estimation for unsaturated flow and transport

394   models — a review. Journal of Hydrology 91(3): 255 – 293.

395 Kulhawy FH (1992) On the evaluation of static soil properties. In Stability and performance of slopes

396   and embankments II, ASCE, pp. 95–115.

397 Leca E and Dormieux L (1990) Upper and lower bound solutions for the face stability of shallow circular

398   tunnels in frictional material. G´eotechnique 40(4): 581–606.

399 Leca E and New B (2007) Settlements induced by tunneling in soft ground. Tunnelling and Underground

400   Space Technology 22(2): 119 – 149.

401 Lee K and Rowe R (1990) Finite element modelling of the three-dimensional ground deformations due

402   to tunnelling in soft cohesive soils: Part i— method of analysis. Computers and Geotechnics 10(2):

403   87 – 109.

404 Lee KM and Rowe RK (1989) Deformations caused by surface loading and tunnelling: the role of elastic

405   anisotropy. Géotechnique 39(1): 125–140.

406 Litwiszyn J (1957) The theories and model research of movements of ground masses. In Proceedings

407   of European Congress Ground Movement, Leeds, Uk, pp. 203–209.

408 Macklin S (1999) The prediction of volume loss due to tunnelling in overconsolidated clay based on

409   heading geometry and stability number. Ground engineering 32(4): 30–33.

410 Maidl B, Herrenknecht M, Maidl U, Wehrmeyer G and Sturge D (2012) Mechanised Shield Tunnelling.

411   John Wiley & Sons.

412 Mair R and Taylor R (1997) Theme lecture: Bored tunnelling in the urban environment. In Proceedings

413   of the fourteenth international conference on soil mechanics and foundation engineering (Hamburg,

414   1997), Balkema, pp. 2353–2385.

415 Mair RJ (2008) Tunnelling and geotechnics: new horizons. Géotechnique 58(9): 695–736.

416 Mair RJ, Gunn MJ and O'Reilly MP (1981) Ground movements around shallow tunnels in soft clay. In

417   Proc. 10th Int. Conf. Soil Mech. and Found. Eng, vol. 1, pp. 323–328.

418 Marshall AM, Farrell R, Klar A and Mair R (2012) Tunnels in sands: the effect of size, depth and volume

419   loss on greenfield displacements. Géotechnique 62(5): 385–399.

420 Meguid M, Saada O, Nunes M and Mattar J (2008) Physical modeling of tunnels in soft ground: A

421   review. Tunnelling and Underground Space Technology 23(2): 185 – 198.

422 Mollon G, Dias D and Soubra AH (2013) Probabilistic analyses of tunneling-induced ground

423   movements. Acta Geotechnica 8(2): 181–199.

424   New BM (1991) Tunnelling induced ground movements: predicting their magnitude and effects. In 4th

425   Int. Conf. Ground Movements and Structures, Pentech Press, pp. 671–697.

426   Osman AS, Bolton MD and Mair RJ (2006) Predicting 2d ground movements around tunnels in

427   undrained clay. Géotechnique 56(9): 597–604.

428   Peck RB (1969) Deep excavations and tunneling in soft ground. In: Proc. 7th International Conference

429   on Soil Mechanics and Foundation Engineering, Mexico City, State of the Art Volume: 225–290.

430   Phoon KK and Kulhawy FH (1999) Characterization of geotechnical variability. Canadian Geotechnical

431   Journal 36(4): 612–624.

432   Pinto F and Whittle AJ (2014) Ground movements due to shallow tunnels in soft ground. i: Analytical

433   solutions. Journal of Geotechnical and Geoenvironmental Engineering 140(4): 04013040.

434   Sagaseta C (1987) Analysis of undraind soil deformation due to ground loss. Géotechnique 37(3): 301–

435   320.

436   Schofield AN (1980) Cambridge geotechnical centrifuge operations. Géotechnique 30(3): 227–268.

437   Suwansawat S and Einstein HH (2006) Artificial neural networks for predicting the maximum surface

438   settlement caused by epb shield tunneling. Tunnelling and Underground Space Technology 21(2):

439   133 – 150.

440   Verruijt A and Booker JR (1996) Surface settlements due to deformation of a tunnel in an elastic half

441   plane. Géotechnique 46(4): 753–756.

442   Vorster TE, Klar A, Soga K and Mair RJ (2005) Estimating the effects of tunneling on existing pipelines.

443   Journal of Geotechnical and Geoenvironmental Engineering 131(11): 1399–1410.

444   Wongsaroj J, Soga K and Mair R (2013) Tunnelling-induced consolidation settlements in london clay.

445   Géotechnique 63(13): 1103–1115.

446   Zhai Q and Rahardjo H (2013) Quantification of uncertainties in soil–water characteristic curve

447   associated with fitting parameters. Engineering Geology 163: 144 – 152.

448

449

450

451

452

453

454   **Notation list**

455   A : is the cross-sectional area of the tunnel.

456   a_S, b_S : are best-fit parameters for the surface settlement curve.

457   a_{S90}, b_{S90} : are best-fit parameters of 90th percentile for the surface settlement curve.

458   a_{S10}, b_{S10} : are best-fit parameters of 10th percentile for the surface settlement curve.

459   a_V, b_V : are best-fit parameters for the volume loss curve.

460   C : is the tunnel cover depth.

461   CoV : is the coefficient of variation.

462   c' : is the effective cohesion.

463   D : is the tunnel diameter.

464   E'_{ur} : is the unloading-reloading elastic modulus for drained condition.

465   E_{ur} : is the unloading-reloading elastic modulus for undrained condition.

466   I : is the point of inflection distance of the settlement trough.

467   k_0 : is the coefficient of lateral earth pressure at rest.

468   L_F : is the load factor.

469   N : is the stability ratio.

470   P : is the applied TBM support pressure.

471   P_0 : is the estimated initial TBM support pressure for face stability.

472   P_{min} : is the minimum applied TBM support pressure before face collapse may occur.

473     $(P_0 - P)_{ult}$: is the ultimate stress difference.

474   R_f : is the constant failure ratio proposed by Duncan and Chang (1970).

475   R^*_f : is a modification of constant failure ratio.

476   S : is the transverse settlement trough curve.

477   S_{max} : is the maximum surface settlement.

478   S_u : is the undrained shear strength.

479   V_L : is the volume loss.

480   γ : is the specific weight.

481   ε : is the axial strain.

482   σ_1 : is the major principal stress.

483   σ_3 : is the minor principal stress.

484   σ_S : is the surcharged load.

485   σ_T : is the tunnel pressure.

486   φ' : is the effective friction angle.

487

488

489

490

491

492

493

494

495

496

497

498

499

500

501

502

503

504

505

506

507

508

509

510

511

512

513

514 **Table captions**

515 Table 1. Data selected from the literature on centrifuge geotechnical tests and reported geotechnical

516 parameters under undrained condition.

517 Table 2. Best-fit and geotechnical parameters under undrained condition, estimated based on the

518 proposed approach.

519 Table 3. Mean and CoV values of maximum surface settlement and applied TBM support pressure

520 between HSP and SCR stations.

521 Table 4. Input geotechnical parameters between HSP and SCR stations (after Franco et al., 2019).

522

523

524 **Figure captions**

525 Figure 1. Typical representation of transverse surface settlement.

526 Figure 2. Sources of longitudinal ground movements due to TBM tunnelling.

527 Figure 3. Comparison of stress paths: a) tunnel excavation producing reduced triaxial extension; b)

528 conventional triaxial compression; c) settlement curve caused by tunneling; d) triaxial loading curve;

529 and e) shear strength envelope.

530 Figure 4. Relationships between maximum surface settlement, S_{max}, and the fitting parameters: a) a_S;

531 and b) b_S.

532 Figure 5. Surface settlement data from Lee and Rowe (1989) and corresponding best-fit modelling.

533 Figure 6. Surface settlement data from Osman et al. (2006) and corresponding best-fit modelling.

534 Figure 7. Surface settlement data for the different forepoling arrangements in centrifuge tests from Divall

535 et al. (2016) and corresponding best-fit modelling: a) FP4 and FP8; b) FP2 and FP6; c) FP5 and FP7;

536 d) FP3 and FP9.

537 Figure 8. Metro stations layout of Line 5.

538 Figure 9. Tunnel model geometry (modified from Franco et al., 2019).

539 Figure 10. Upper and lower bounds of S_{max} between stations HSP and SCR.

540

541

542

543

544

545 **Tables**

546 Table 1. Data selected from the literature on centrifuge geotechnical tests and reported geotechnical parameters under undrained condition.

Reference	Test ID	(C/D)	D (mm) [m]*	Scale Factor N	Geotechnical parameters	
					E_{ur} (kPa)	S_u (kPa)
Lee and Rowe (1989)	2DP	1.67	36 [4.5]	125	3640	25.3
	2DH	1.80	60 [4.5]	75	-	26.0
Osman *et al.,* (2006)	2DP	1.67	60 [4.5]	75	-	22.6
	2DT	1.67	36[4.5]	125	-	22.6
	FP2				-	33.7
	FP3				-	30.7
	FP4				-	35.0
	FP5				-	34.3
Divall *et al.,* (2016)	FP6	2.00	50 [5.0]	100	-	32.8
	FP7				-	33.1
	FP8				-	32.1
	FP9				-	35.3

* The values in brackets correspond to the full-scale diameter, in meters.

547

548

549

550

551

552

553

554   Table 2. Best-fit and geotechnical parameters under undrained condition, estimated based on the proposed approach.

Reference	Test ID	R_f^*	Best-fit parameters		n	Standard Error (SE)		R^2	RMSE	Geotechnical parameters	
			a_SD	b_S		P (kPa)	S_{max} (mm)			E_{ur} (kPa)	S_u (kPa)
Lee and Rowe (1989)	2DP	0.54	0.01040	0.01180	21	4.5934	0.3751	0.993	0.142	3462	22.8
Osman *et al.* (2006)	2DH	0.50	0.01690	0.01050	8	7.9040	0.5666	0.988	0.151	3550	23.8
	2DP	0.54	0.01740	0.01190	20	4.7783	0.6407	0.995	0.198	3448	22.6
	2DT	0.54	0.00890	0.01355	18	4.4887	0.3796	0.988	0.171	4045	19.9
Divall *et al.* (2016)	FP2	0.45	0.00422	0.00665	115	3.4845	0.0877	0.996	0.056	11848	33.8
	FP3		0.00525	0.00699	94	3.6095	0.1039	0.994	0.079	4762	32.2
	FP4		0.00395	0.00715	65	4.6069	0.1523	0.833	0.497	12658	31.5
	FP5		0.00199	0.00568	141	4.8731	0.1676	0.915	0.577	25126	39.6
	FP6		0.00525	0.00722	74	4.2731	0.1440	0.993	0.102	9524	31.2
	FP7		0.00118	0.00596	155	3.6571	0.0320	0.966	0.074	42373	37.1
	FP8		0.00655	0.00687	112	3.3305	0.0942	0.994	0.076	7634	32.8
	FP9		0.00545	0.00602	70	4.8642	0.1302	0.995	0.074	9174	37.4

555

556

557

558

559

560

561

562

563   Table 3. Mean and CoV values of maximum surface settlement and applied TBM support pressure between HSP and SCR stations.

Section number	Monitoring sections	S_{max} (mm)	P (kPa)
1	SC_19+138	1.6	224.00
2	SC_19+162	1.6	237.00
3	SC_19+187	2.3	239.00
4	SC_19+210	1.9	265.00
5	SC_19+234	0.6	260.00
6	SC_19+260	0.7	246.00
7	SC_19+336	3.5	211.00
8	SC_19+400	4.7	199.00
9	SC_19+415	3.5	199.00
10	SC_19+438	3.0	203.00
11	SC_19+461	2.6	207.00
12	SC_19+486	2.7	215.00
13	SC_19+512	3.5	227.00
14	SC_19+560	1.4	238.00
15	SC_19+581	1.6	235.00
16	SC_19+634	3.4	249.00
17	SC_19+658	4.0	239.00
18	SC_19+682	4.8	240.00
19	SC_19+708	3.7	232.00
μ		2.7	229.74
σ		1.3	19.66
CoV	(%)	48.15	8.56

564

565

566

567   Table 4. Input geotechnical parameters between HSP and SCR stations (after Franco et al., 2019).

Geotechnical parameters		$3A_{gp1}$	$3A_{g1.2}$	$3A_{r1.2}$	$4A_{g1}$
γ	kN/m^3	16.6	18.5	19.5	20.2
c'	kPa	18	40	7	80
j'	deg	24	24	32	26
E	MPa	20	120	185	230
n	-	0.26	0.30	0.31	0.28
k_0	-	0.67	0.93	0.82	0.90

568

569

570 **Figures**

571 Figure 1. Typical representation of transverse surface settlement.

572

573

574 Figure 2. Sources of longitudinal ground movements due to TBM tunnelling.

575

576

577

578

579

580

581

582

583

584

585

586

587

588

589

590

591

592

593

594 Figure 3. Comparison of stress paths: a) tunnel excavation producing reduced triaxial extension; b)
595 conventional triaxial compression; c) settlement curve caused by tunneling; d) triaxial loading curve;
596 and e) shear strength envelope.

(a)   (b)

(c)   (d)

597

(e)

598

599 Figure 4. Relationships between maximum surface settlement, S_{max}, and the fitting parameters: a) a_S;

600 and b) b_S.

601

602   (a)   (b)

603

604

605 Figure 5. Surface settlement data from Lee and Rowe (1989) and corresponding best-fit modelling.

606
607

608 Figure 6. Surface settlement data from Osman et al. (2006) and corresponding best-fit modelling.

609
610
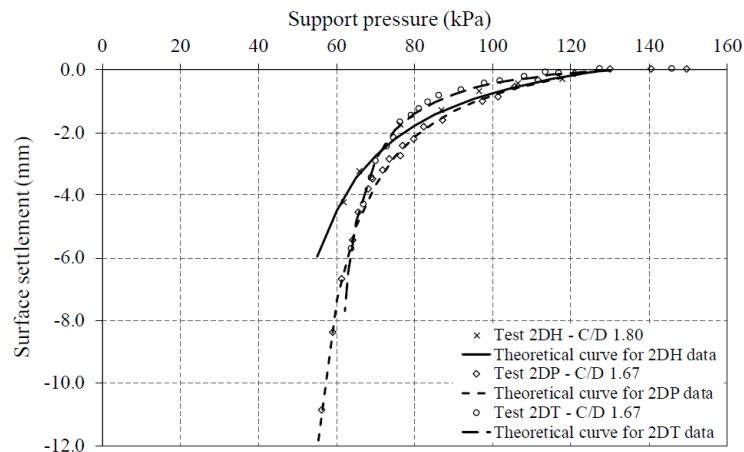611
612
613
614
615
616
617
618
619
620
621

622   Figure 7. Surface settlement data for the different forepoling arrangements in centrifuge tests from Divall

623   et al. (2016) and corresponding best-fit modelling: a) FP4 and FP8; b) FP2 and FP6; c) FP5 and FP7;
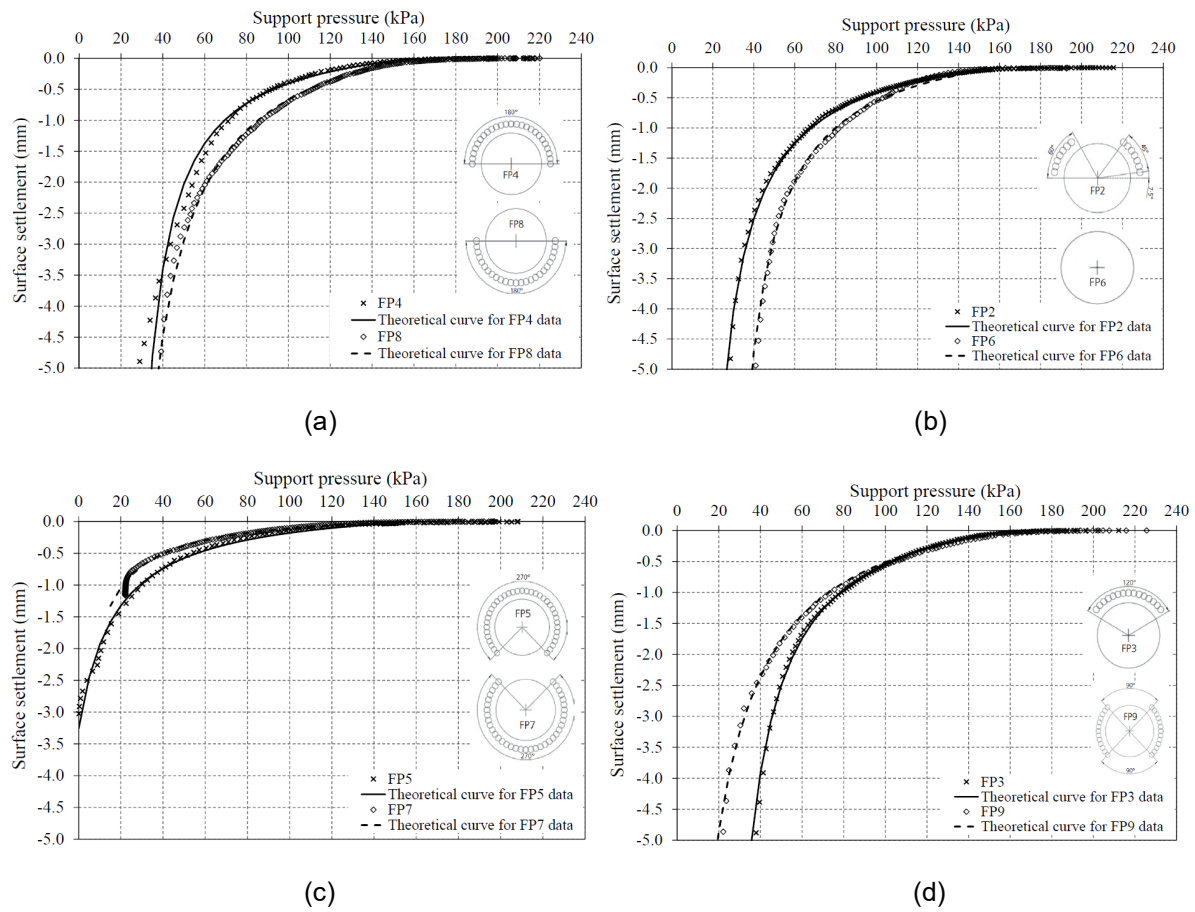
624   d) FP3 and FP9.

625

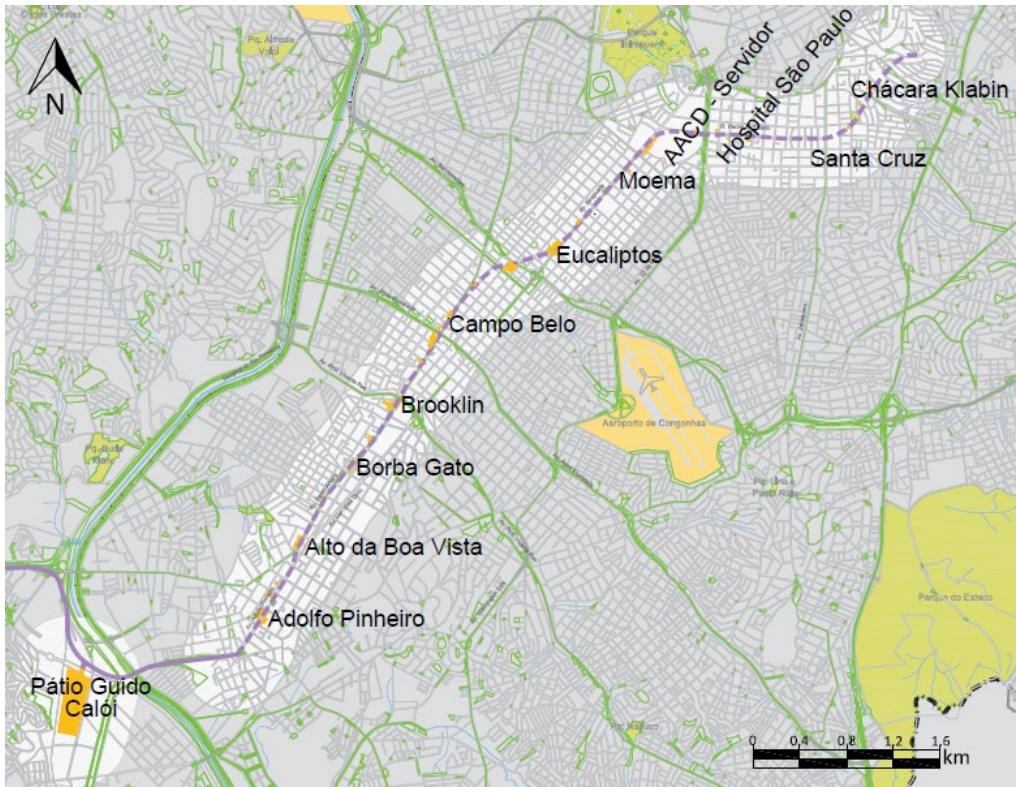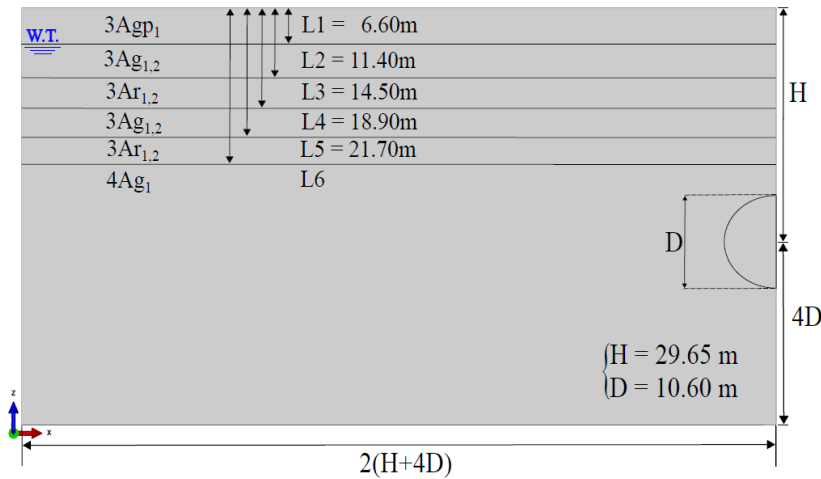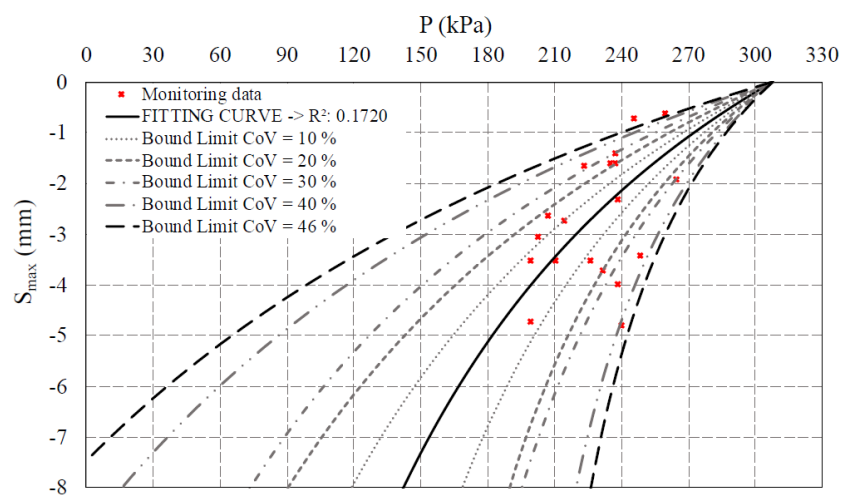626   (a)   (b)

627

628   (c)   (d)

629

630

631

632

633

634

635

636

637

638

639

640

641   Figure 8. Metro stations layout of Line 5.

642

643

644

645   Figure 9. Tunnel model geometry (modified from Franco et al., 2019).

646

647

648

649

650

651

652   Figure 10. Upper and lower bounds of S_{max} between stations HSP and SCR.

653
654